Numerical Simulation of the Nocturnal Turbulence Characteristics over Rattlesnake Mountain*

W. E. HEILMAN

USDA Forest Service, North Central Forest Experiment Station, East Lansing, Michigan

E. S. TAKLE

Department of Geological and Atmospheric Sciences, Iowa State University, Ames, Iowa

(Manuscript received 15 October 1990, in final form 4 March 1991)

ABSTRACT

A two-dimensional second-order turbulence-closure model based on Mellor–Yamada level 3 is used to examine the nocturnal turbulence characteristics over Rattlesnake Mountain in Washington. Simulations of mean horizontal velocities and potential temperatures agree well with data. The equations for the components of the turbulent kinetic energy (TKE) show that anisotropy contributes in ways that are counter to our intuition developed from mean flow considerations: shear production under stable conditions forces the *suppression* of the vertical component proportion of total TKE, while potential-temperature variance under stable conditions leads to a positive (countergradient) contribution to the heat flux that *increases* the vertical component proportion of total TKE. This paper provides a qualitative analysis of simulated turbulence fields, which indicates significant variation over the windward and leeward slopes. From the simulation results, turbulence anisotropy is seen to develop in the katabatic flow region where vertical wind shears and atmospheric stability are large. An enhancement of the vertical component proportion of the total TKE takes place over the leeward slope as the downslope distance increases. The countergradient portion of the turbulent heat flux plays an important role in producing regions of anisotropy.

1. Introduction

There have been numerous studies, both field and numerical, that examine boundary-layer variables over nonhomogeneous terrain under stable conditions. Manins and Sawford (1979a) used a hydraulic model to show the importance of interfacial mixing in the growth of katabatic flow. Rao and Snodgrass (1981) presented a nonstationary one-dimensional model to study the equilibrium structure of katabatic flow. Garrett (1983) and Heilman and Dobosy (1985) incorporated canopy, soil, and radiation parameterizations in one-dimensional models to study katabatic flow. Two- and three-dimensional models have been used by Yamada (1981, 1983), Garrett and Smith (1984), McNider and Pielke (1984), Nappo and Rao (1987), Bader et al. (1987), Leone and Lee (1989), and Yamada and Bunker (1989) to study drainage flows over various complex terrain features. Field studies of nocturnal conditions over complex terrain have been reported by Manins and Sawford (1979b), Doran and Horst (1983), Gudiksen (1983), Horst and Doran (1982, 1986), Whiteman and Barr (1986), Doran et al. (1989), Clements et al. (1989), Stone and Hoard (1989), and Shinn et al. (1989).

Many of the previous studies have concentrated on simulating and measuring mean fields. Most models are able to simulate mean fields adequately. However, the turbulence structure over nonhomogeneous terrain in stable conditions has not been extensively reported in the literature. Unfortunately, field measurements of turbulence structure over nonhomogeneous terrain are limited. This does not allow for extensive model verification. Nevertheless, turbulence modeling should at least qualitatively provide some insight into how terrain features affect the turbulence structure under stable conditions.

In this study, the level-3 turbulence scheme of Mellor and Yamada (1974) is used to simulate the mean and turbulence field over Rattlesnake Mountain, and the results are compared to observations wherever possible. This scheme is relatively simple, but does allow for a limited degree of anisotropy. Yamada (1983) used level 2.5 to simulate conditions at Rattlesnake Mountain. We have extended his work and evaluated the turbulence structure at this site.

* Journal Paper No. J-13054 of the Iowa Agriculture and Home Economics Experiment Station, Ames, IA. Project No. 2779.

Corresponding author address: Dr. W. E. Heilman, USDA Forest Service, North Central Forest Experiment. Station, 14075. Harrison Road, East Lansing, MI 48823.

2. Model overview

Mellor and Yamada (1974) presented a four-level hierarchy for turbulence closure applicable to boundary-layer processes. The attractiveness of level 3 of this hierarchy, which is used in this study, is that some departure from turbulence isotropy is allowed, and yet the scheme is significantly less complicated than the full mean Reynolds stress equations of level 4. The turbulence portion of the level-3 model consists of prognostic equations for turbulent kinetic energy (TKE), length scale, and virtual potential temperature variance, while diagnostic equations are incorporated for all other turbulent quantities. Mean variables predicted by the level-3 model include the horizontal wind components and virtual potential temperature. Vertical wind speeds are computed from the incompressible form of the continuity equation. Simulation of the ground surface cooling is accomplished through the use of the force–restore method of Deardorff (1978). A complete listing of the model equations can be found in Heilman (1988).

The two-dimensional form of the boundary-layer equations used in the present model is transformed to a nonorthogonal terrain-following coordinate system, with the modified height coordinate given by

$$s - \frac{z - z_g(x)}{H - z_g(x)}, \tag{1}$$

where z is the Cartesian height, $z_g(x)$ is the height of the ground above some reference, x is the horizontal distance from some reference point, and H is the height of the model top. The general transformation equations of Kasahara (1974) are employed, where only variations in the s and x directions are allowed.

The two-dimensional level-3 diagnostic equations for the TKE components, momentum fluxes, and turbulent fluxes are given by

$$\begin{pmatrix} \overline{u'^2} \\ \overline{v'^2} \\ \overline{w'^2} \end{pmatrix} = \frac{q^2}{3}\begin{pmatrix} 1 \\ 1 \\ 1 \end{pmatrix} + \frac{l_1}{q}\begin{pmatrix} -4P_{xx} + 2P_{yy} - 2\beta g\overline{w'\theta'_v} \\ 2P_{xx} - 4P_{yy} - 2\beta g\overline{w'\theta'_v} \\ 2P_{xx} + 2P_{yy} + 4\beta g\overline{w'\theta'_v} \end{pmatrix} \tag{2}$$

$$\begin{pmatrix} \overline{u'v'} \\ \overline{u'w'} \\ \overline{v'w'} \end{pmatrix} = \frac{3l_1}{q} \times \begin{pmatrix} -P_{yx} - P_{xy} \\ -(\overline{w'^2} - c_1q^2)(\partial U/\partial s)(H - z_g)^{-1} + \beta g\overline{u'\theta'_v} \\ -(\overline{w'^2} - c_1q^2)(\partial V/\partial s)(H - z_g)^{-1} + \beta g\overline{v'\theta'_v} \end{pmatrix} \tag{3}$$

$$\begin{pmatrix} \overline{u'\theta'_v} \\ \overline{v'\theta'_v} \\ \overline{w'\theta'_v} \end{pmatrix} = \frac{3l_2}{q} \times \begin{pmatrix} -(\overline{u'w'})(\partial\Theta_v/\partial s)(H - z_g)^{-1} - (\overline{w'\theta'_v})(\partial U/\partial s)(H - z_g)^{-1} \\ -(\overline{v'w'})(\partial\Theta_v/\partial s)(H - z_g)^{-1} - (\overline{w'\theta'_v})(\partial V/\partial s)(H - z_g)^{-1} \\ -(w'^2)(\partial\Theta_v/\partial s)(H - z_g)^{-1} + \beta g\theta'^2_v \end{pmatrix} \tag{4}$$

$$P_{ij} = \frac{\overline{u'_i w'}}{(H - z_g)}\frac{\partial U_j}{\partial s}. \tag{5}$$

A complete list of symbols can be found in the Appendix.

Equation (2) describes the effects of mechanical production of turbulence and turbulent heat flux on turbulence isotropy. The anisotropic terms contribute to the components of TKE in ways that are counter to our intuition developed from mean flow considerations. For example, large shears under stable conditions force the *suppression* of the vertical component proportion of the total TKE. This redistribution has no effect on the total TKE, since the sum of the terms in brackets in Eq. (2) is zero. However, as can be seen from Eqs. (3) and (4), this anisotropy in the TKE (more specifically, the modification of $\overline{w'^2}$) does create changes in the modeled vertical fluxes of momentum and heat. The quantity P_{xx} becomes large negative under strong shear. This increases u'^2 [through the first component of Eq. (2)] and decreases w'^2 [through the third component of Eq. (2)]. The decreased w'^2 reduces the vertical fluxes of both momentum [second and third components of Eq. (3)] and heat [third component of Eq. (4)]. The level-3 scheme of Mellor–Yamada also allows for a potential temperature variance contribution to the heat flux that is of opposite sign to the contribution from the mean gradient under stable conditions. This could lead to a countergradient heat flux if the last term in the third component of the rhs of Eq. (4) is larger than the first term. Such a countergradient term would arrest the decrease of w'^2 through the last term in Eq. (2).

Nocturnal drainage flows are prime examples of anisotropic conditions created by large shears in horizontal velocity. Such flows then would create vertical fluxes of momentum and heat that would be less than expected if the fluxes were modeled by use of a turbulent diffusivity that depends only on the total TKE (e.g., Garrett 1983; Bader et al. 1987).

3. Computational processes

Rattlesnake Mountain, located in south-central Washington, is a nearly two-dimensional ridge oriented

from northwest to southeast. The ridge characteristics and experimental data have been compiled by Horst and Doran (1982). Data collected on the night of 1 July 1980 from three meteorological towers and a tethersonde were used for model comparisons. The slope of the terrain varied from 21° at towers A and B to 8° at tower C (see Fig. 1). The computational domain spans a 5.58 × 1.1 km^2 region. The horizontal grid spacing for the model is set at 180 m, and the vertical grid spacing is constant near the surface and log-linear above. Near the surface, the vertical grid spacing is approximately 2 m. The grid is staggered in the vertical, with the velocity components calculated at grid points between those used for calculating all other variables (Heilman 1984). An alternating-direction–implicit method (Polezhaev 1967) is used to solve the atmospheric governing equations at the interior grid points.

The use of a hydrostatic model with relatively fine grid resolution to simulate atmospheric conditions over terrain with slope angles similar to those encountered on Rattlesnake Mountain must be done carefully. Song et al. (1985) have shown the importance of nonhydrostatic effects when simulating atmospheric features with small-length scales. However, nonhydrostatic effects were also shown to be much less significant when atmospheric stability increases. The conditions simulated in this study are characterized by extreme stability in the inversion layer. Although the grid spacing is set at 180 m and the maximum slope angle of the constant height surfaces is 21°, the significant stability in the low-level inversion layer will mitigate, to a large extent, the nonhydrostatic effects. Many of the previous simulations of drainage flow conditions over complex terrain have, in fact, been hydrostatic (Yamada 1981, 1983; Garrett and Smith, 1984; McNider and Pielke 1984; Yamada and Bunker 1989).

Inflow and outflow lateral boundary conditions are specified, with the one-dimensional version of the model equations used at the inflow boundary. Neucmann conditions are specified at the top boundary for U, V, Θ_v, and l, while q^2 and $\overline{\theta_v'^2}$ are set at 0.0001 m^2 s^{-2} and 0.0 K^2, respectively, at the model top. The pressure gradient in the model is expressed in terms of geostrophic wind components U_g and V_g that are given values of 2.8 m s^{-1} and 0.0 m s^{-1}, respectively, at the model top. These values are in accordance with the measured data. Implied in these values is the alignment of the x axis with the geostrophic wind direction of 225°. Bottom boundary conditions for the model are based on the work of Businger et al. (1971), Mellor and Yamada (1974), and Deardorff (1978).

Initial conditions for the mean quantities are obtained from the 1 July 1980 tethersonde data centered at 2000 PST. The initial wind field at the tethersonde site is assumed to be logarithmic from the ground up to the level where it matches the geostrophic wind, with $u_* = 0.2$ m s^{-1} and $z_0 = 0.03$ m. The wind speeds at other locations are scaled to conserve mass. The initial vertical potential temperature field is assumed constant; $\Theta_v = 305.3$ K. Initial conditions for q^2, l, $\overline{\theta_v'^2}$ are obtained from the diagnostic relations of level 2 of the Mellor–Yamada hierarchy (Yamada 1975; Yamada 1983).

The model was run with a 10-s time step for a 3-h period, beginning at 2000 PST and ending at 2300 PST. The presented results correspond to 2300 PST.

4. Numerical results

a. Mean velocities

Figure 1 shows the entire simulated velocity field over Rattlesnake Mountain at 2300 PST. A very shallow drainage layer exists on both sides of the ridge, with flow reversal occurring on the windward side. The conspicuous vertical velocities near the model top result from the use of the transformed incompressible continuity equation, with no adjustment at the model top.

Profiles of horizontal velocity within the drainage layer are shown in Fig. 2. On the windward side of the ridge, negative velocities occur at horizontal locations of $x < 2.34$ km. Above this region of negative velocities, the vertical shears are large as the U velocities increase with height toward the ambient conditions. On the leeward side of the ridge, a maximum speed of approximately 3.4 m s^{-1} occurs at $x = 4.50$ km. The depth of the drainage layer and the levels of the speed maxima increase with increasing distance from the ridge top. The structure of the induced katabatic flow on both sides of the ridge is agrees with results of Arritt and Pielke (1986), who found induced katabatic flow to be stronger and exist at a lower height with an opposing ambient wind than with a following ambient wind. Chang et al. (1982) observed an analogous phenomenon in the simulation of a coastal area, where an opposing synoptic wind strengthened and lowered the

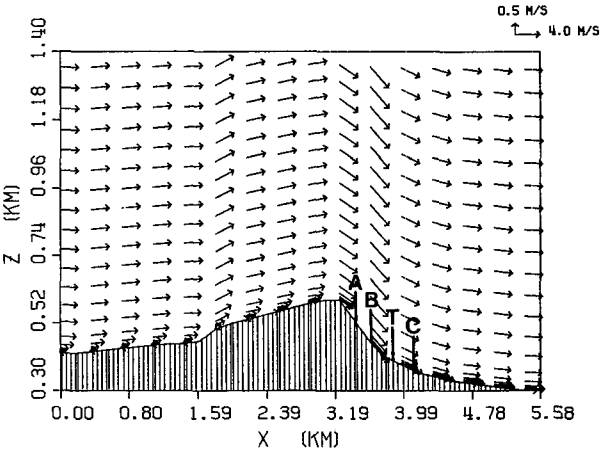

FIG. 1. Simulated velocities over Rattlesnake Mountain at 2300 PST 1 July 1980. Tower locations are indicated by A, B, and C and tethersonde location is indicated by T.

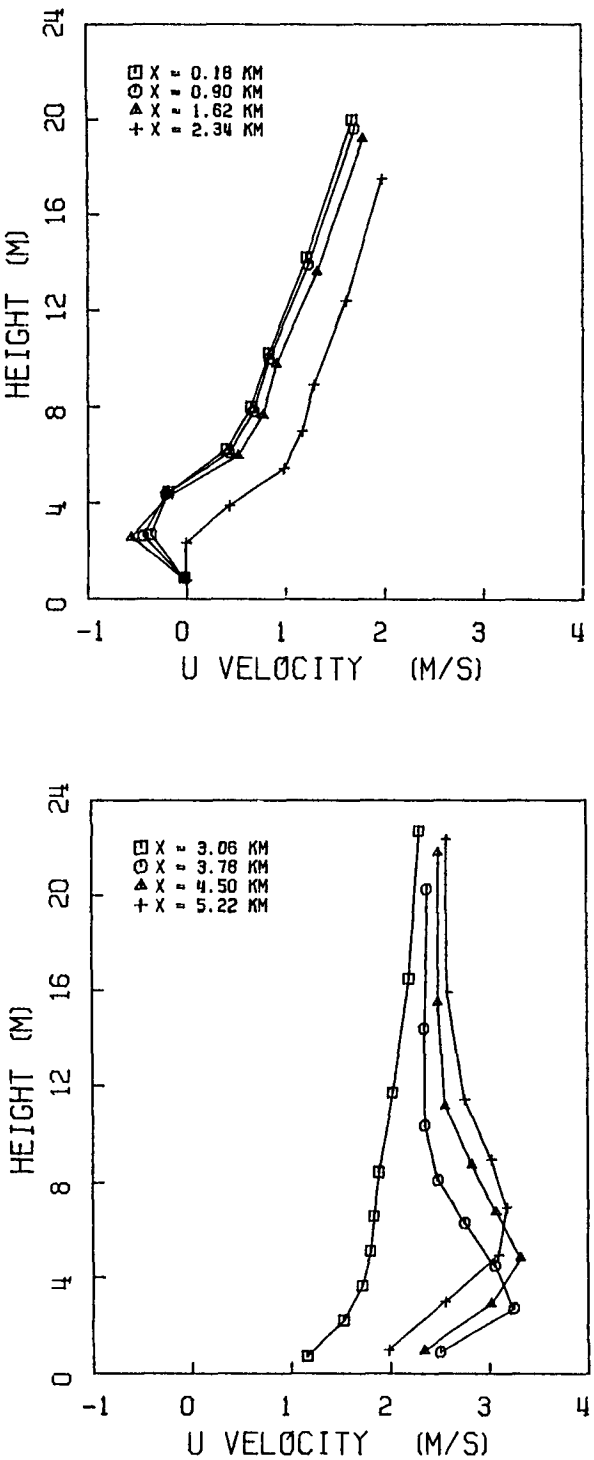

FIG. 2. Simulated U-velocity profiles at eight locations over Rattlesnake Mountain at 2300 PST 1 July 1980.

wind maximum in a sea-breeze simulation. On the windward side of the ridge, the drainage-layer depth is quite uniform, and the maxima always occur very close to the surface. On the other hand, the leeward drainage depth does not remain uniform but increases with increasing downslope distance. The difference between the induced katabatic flow and the ambient flow is much stronger on the windward side of the ridge. As a result, mechanical production of turbulence above the drainage layer should be much larger on the windward side.

Comparisons of the simulated mean velocities with the measured velocities at towers B and C are shown in Fig. 3. The tower data, reported every 10 min, have been averaged over a 1-h period from 2230 to 2330 PST. Both profiles compare quite favorably with the data.

b. Mean potential temperature

The potential temperature profiles are shown in Fig. 4. Radiational cooling of the surface produces a low-level inversion layer. All the windward profiles in this inversion layer are very similar. On the leeward side, however, the coldest air exists at large distances from the ridge top. There is enhanced stability at a height of 4–8 m above the surface on the leeward side of the ridge top in comparison with the windward side. The maximum lapse rate in this region is about 1 K m^{-1} over the leeward slope and 0.5 K m^{-1} over the windward slope. This increased stability affects the turbulence structure by increasing the buoyant dissipation. The vertical extent of the enhanced stability increases with x on the leeward side, with the strongest stability occurring over the steepest portion of the leeward slope.

Comparisons of model results with the observed potential temperature profiles at the tower and tethersonde sites are shown in Fig. 5. The model predictions show reasonable agreement with the data. Small differences in the profiles can be expected because the virtual potential temperature field initially was set to a constant value obtained from an analysis of the upper-level potential temperature and mixing ratio profiles at the tethersonde site. Actual potential temperature profiles at the tower and tethersonde sites indicate nonhomogeneous and slightly stable conditions near the surface.

c. Turbulence

The simulated mean velocities and virtual potential temperatures result in a simulated turbulence structure that exhibits some interesting features. For example, the TKE profiles shown in Fig. 6 indicate marked differences over the windward and leeward slopes. It is noteworthy that TKE maxima over the windward slope are elevated and do not exist at precisely the same height as the wind shear maxima (see Fig. 2). An analysis of the mechanical production of TKE ($\overline{u'w'}\partial U/\partial s$) indicates that production has a relative maximum at the same height as the TKE maximum. Figure 7 clearly shows that the absolute values $\overline{u'w'}$ are

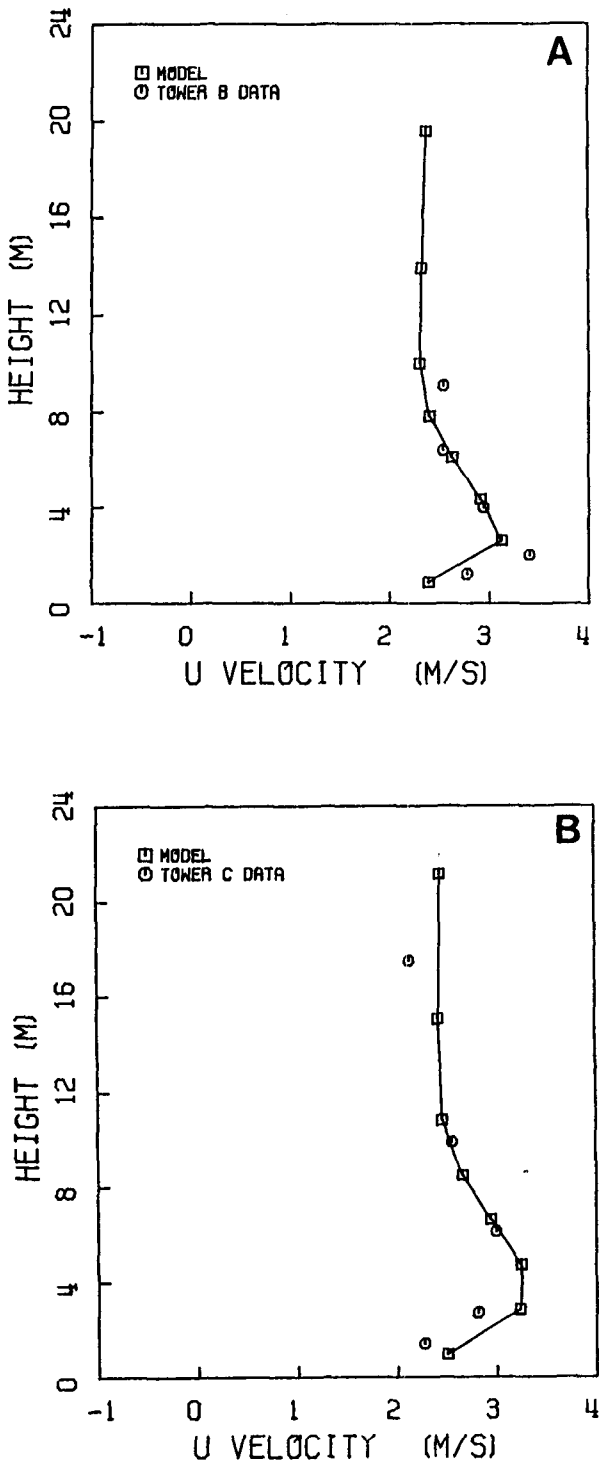

FIG. 3. Simulated and measured U-velocity profiles (a) at tower B and (b) at tower C on Rattlesnake Mountain at 2300 PST 1 July 1980.

largest at nearly the same elevations as the maxima in the TKE profiles over the windward slope, although the TKE profiles are smoother and show less distinct maxima. Obviously, both the Reynolds stress and vertical wind shear play a role in determining the structure of mechanical production, and they may not necessarily reach a maximum at the same level. According

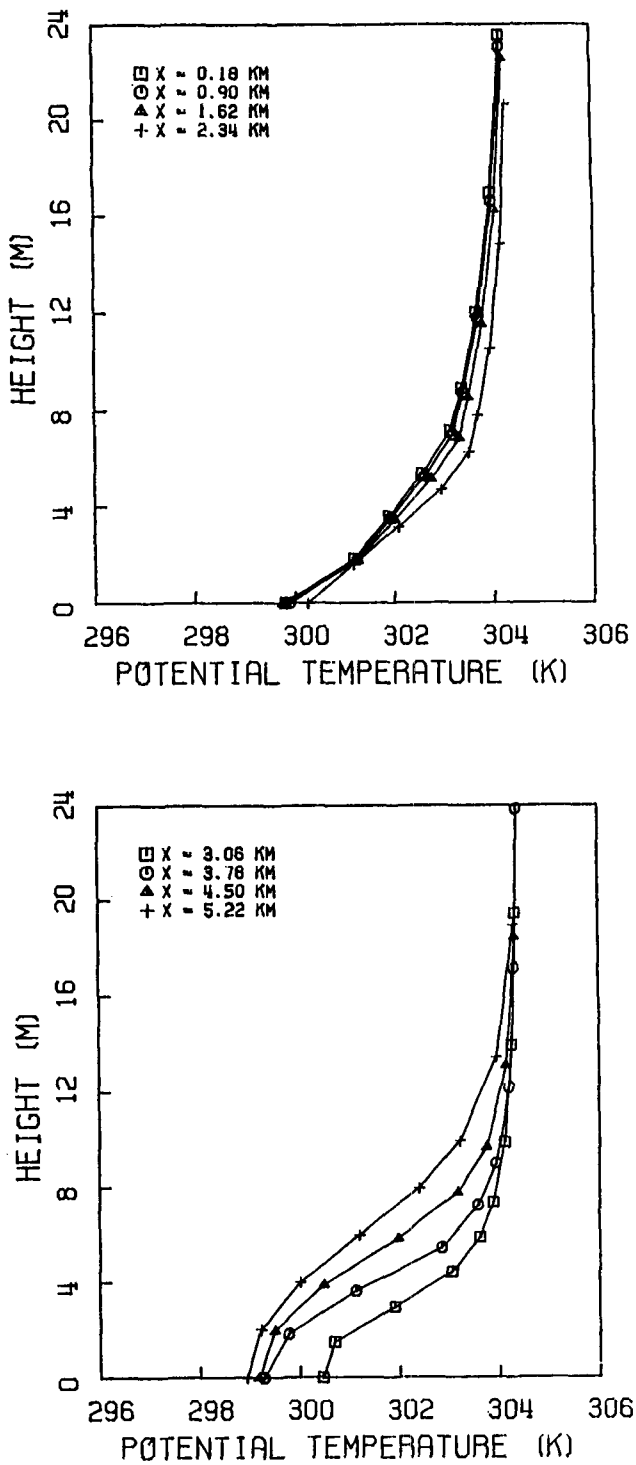

FIG. 4. Simulated potential temperature profiles at eight locations over Rattlesnake Mountain at 2300 PST 1 July 1980.

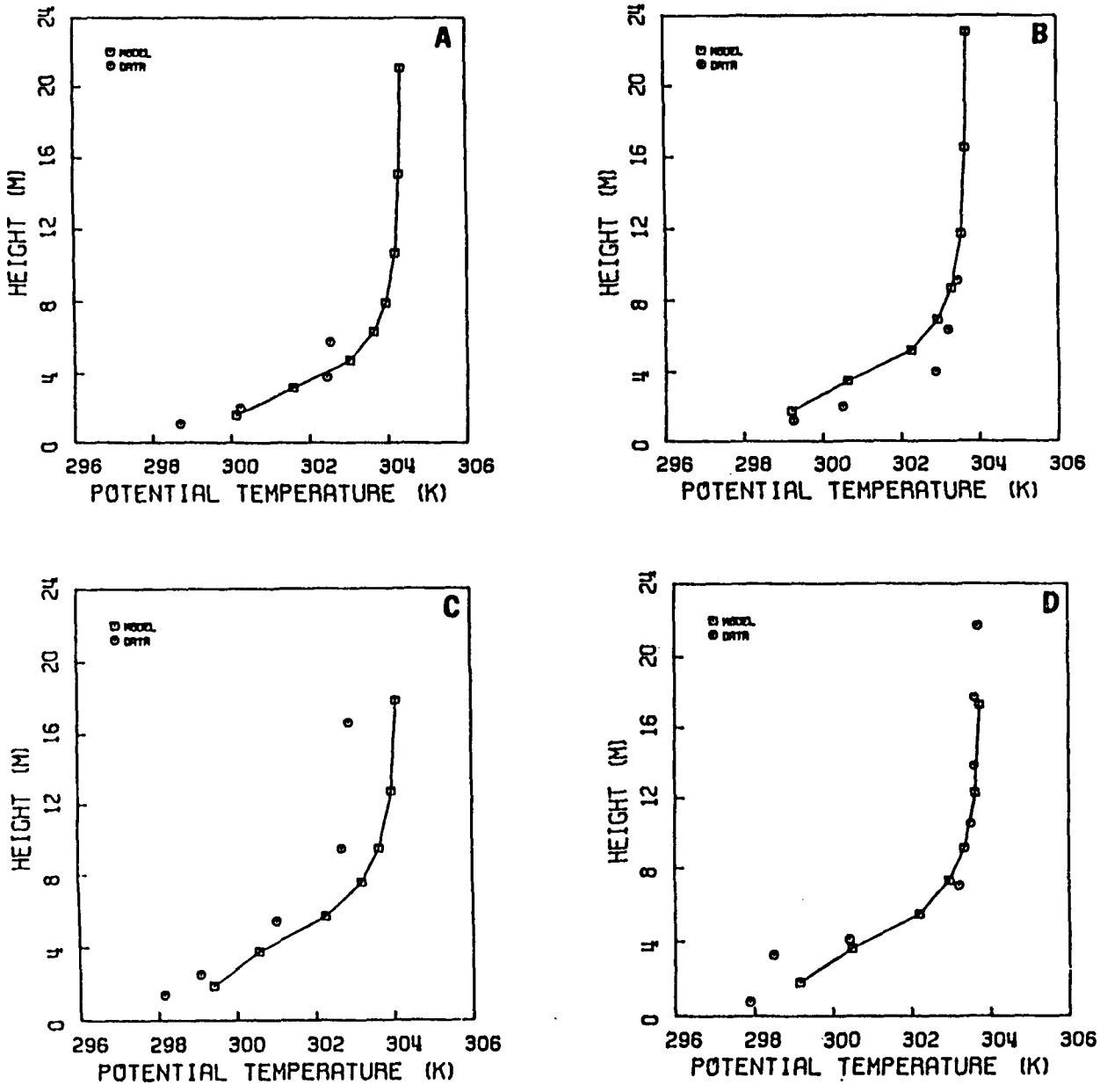

FIG. 5. Simulated and measured potential temperature profiles (a) at tower A, (b) at tower B, (c) at tower C, and (d) at the tethersonde site on Rattlesnake Mountain at 2300 PST 1 July 1980

to Eq. (3), the Reynolds stress is dependent on the vertical component of TKE as well as the total TKE. Thus, departures from turbulence isotropy affect the profiles of Reynolds stress and the associated profiles of mechanical production of TKE. If the Reynolds stress is parameterized in terms of the vertical wind shear and an eddy diffusivity dependent on the total TKE (e.g., Garrett 1983), the region of maximum TKE under stable conditions should exist very close to the region of maximum vertical wind shear and mechanical production. Second- and higher-order closure models allow for the calculation of Reynolds stresses independent of any constraints of prescribed eddy diffusivities. Such models reveal the role of anisotropic effects on the total turbulence structure.

On the leeward side of the ridge, TKE maxima exist just above the surface where, in this case, the vertical wind shear is the strongest. Above the drainage flow maxima (10 m), the TKE is about 50% less than the TKE over the windward slope at the same height above

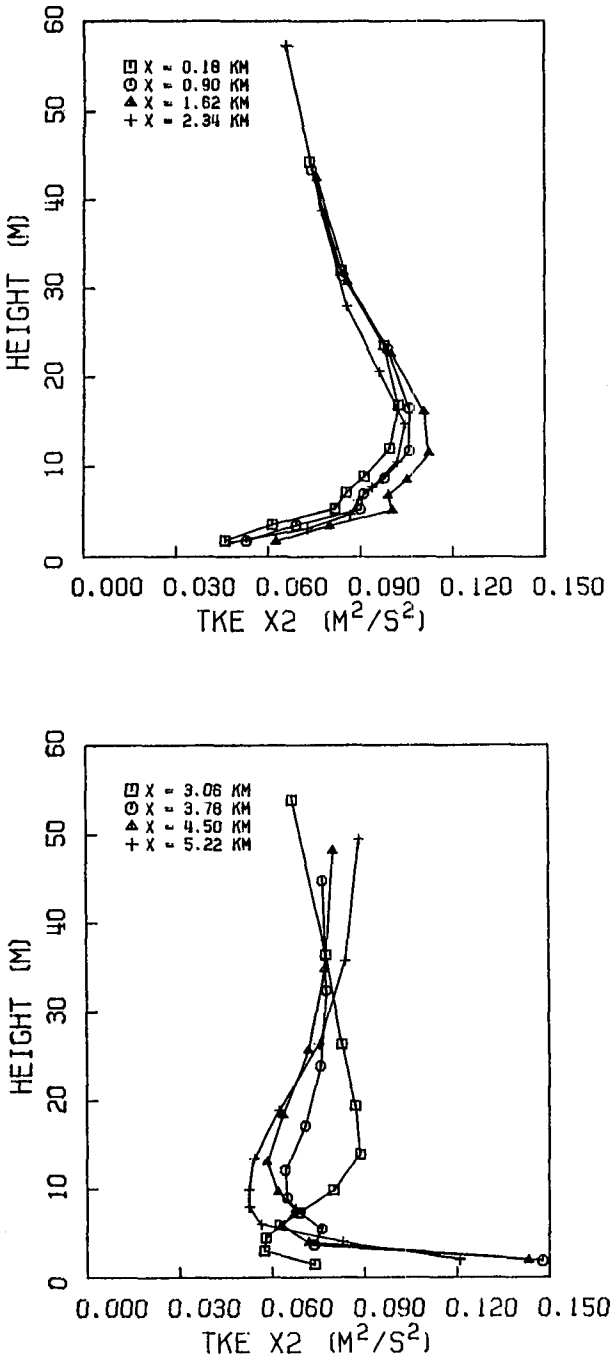

FIG. 6. Simulated turbulent kinetic energy profiles at eight locations over Rattlesnake Mountain at 2300 PST 1 July 1980.

the surface. The suppression of TKE in this region is related to the reduced vertical wind shear and Reynolds stress in this region (see Figs. 2 and 7). Because the ambient flow does not oppose the drainage flow over the leeward slope, there is a reduction in the product of Reynolds stress and vertical wind shear above the drainage flow maxima. This prevents mechanical production of TKE from playing a major role in this region.

The lack of turbulence data over Rattlesnake Mountain does not allow for model verification of turbulence results. However, the TKE values obtained in

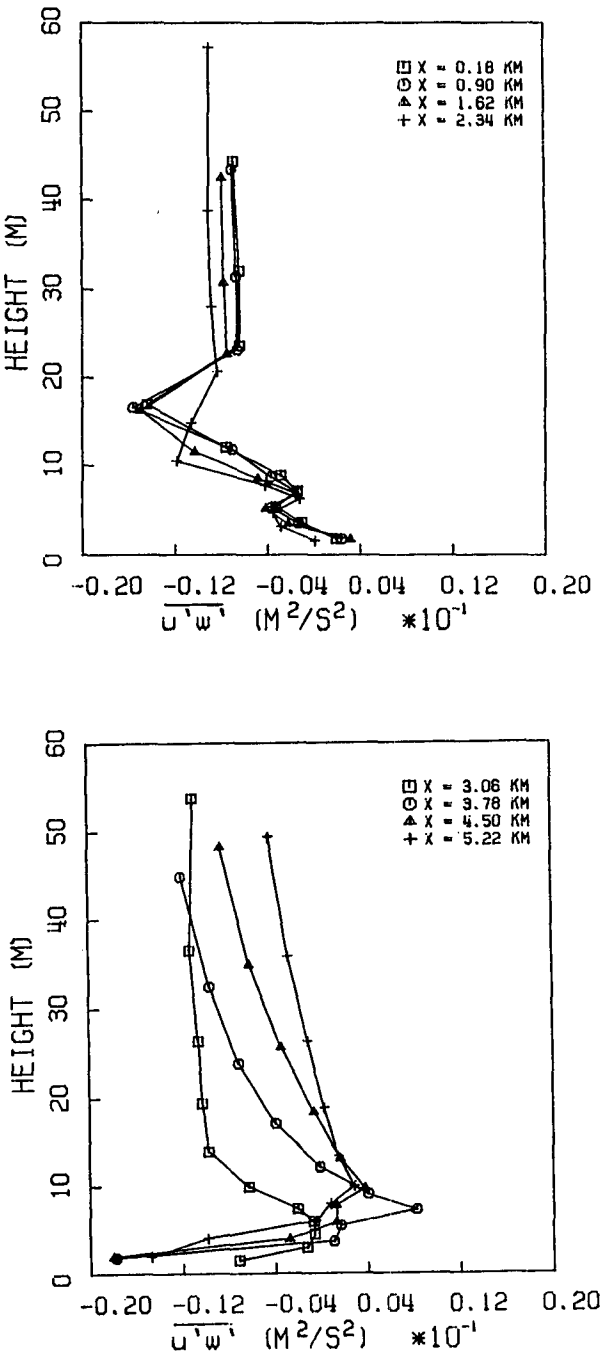

FIG. 7. Simulated Reynolds stress profiles at eight locations over Rattlesnake Mountain at 2300 PST 1 July 1980.

this simulation are similar to the model and experimental data of Yamada and Bunker (1989) and Shinn et al. (1989).

Another interesting feature of the turbulence structure is the behavior of the vertical turbulent heat flux over the windward and leeward slopes, as shown in Fig. 8. All the windward profiles are very similar; however, the leeward profiles show much more spatial variability. The contribution of the countergradient heat flux component ($3l_2\beta g\theta_v'^2/q$) in the expression for the vertical heat flux [see Eq. (4)] results in regions within the inversion layer having upward fluxes. The reason for the variability is that the simulated virtual potential temperature variances are nearly twice as large over the leeward slope in the drainage layer. The large variances increase sufficiently the countergradient portion of the turbulent heat flux to cause the heat fluxes to be quite variable and certainly more positive than if the gradient portion acted alone.

The simulated horizontal heat flux $\overline{u'\theta_v'}$ over the leeward slope (not shown) takes on positive values below the drainage flow maxima and negative values above. This is consistent with the data obtained by Horst and Doran (1988). Over the windward slope, simulated values of $\overline{u'\theta_v'}$ are negative below the drainage flow maxima and positive above.

The model prediction of $\overline{u'\theta_v'}/\overline{w'\theta_v'}$ on both sides of the ridge top where $\overline{w'\theta_v'}$ is negative yields values near 2.5 just above the drainage flow maxima, increasing to about 4.0 near the top of the drainage layer. These values are similar to the data analyzed at Cabauw, The Netherlands, by Nieuwstadt (1984). Data obtained by Horst and Doran (1988) over Rattlesnake Mountain indicate similar values, but the values decrease in magnitude as values of distance above the slope normalized by a local Obukhov length increase.

As noted in the discussion of the TKE structure, the product of $\overline{u'w'}$ and $\partial U/\partial s$ determines the mechanical production of TKE. Large stresses in the inversion layer tend to suppress values of $\overline{w'^2}/q^2$ and enhance $\overline{u'^2}/q^2$ [see Eq. (2)]. Profiles of $\overline{w'^2}q^2$ are shown in Fig. 9. The minima in the $\overline{w'^2}/q^2$ profiles over the windward slope occur at the same heights where the mechanical production values are large. Over the leeward slope, the suppression of $\overline{w'^2}/q^2$ values is observed near the drainage flow maxima where the Reynolds stresses and mechanical production of TKE are very small. Even though the Reynolds stress is relatively weak at those levels, the increased stability there is sufficient to force significant anisotropy.

Above the drainage layer over the leeward slope, $\overline{w'^2}/q^2$ values tend to increase as x increases. There are two mechanisms responsible for this phenomenon. The first mechanism is the decrease in absolute value of the Reynolds stress above 10 m as x increases (see Fig. 7). This decrease in the downward flux of momentum tends to reduce the mechanical production

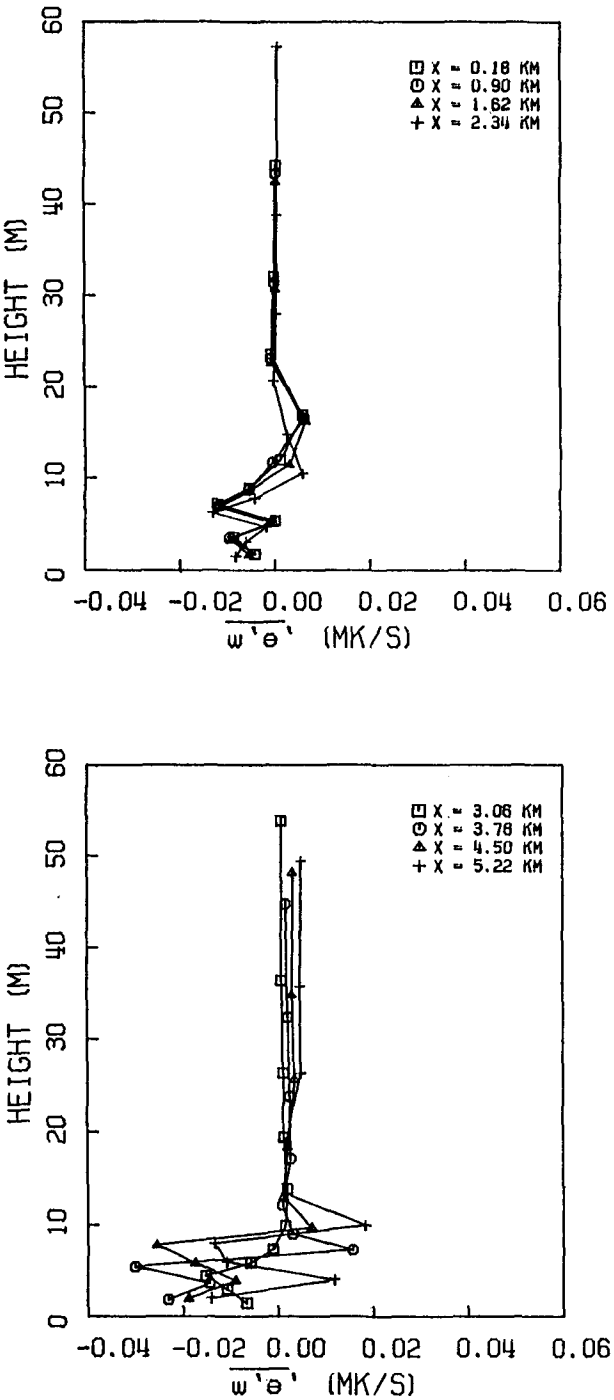

FIG. 8. Simulated vertical turbulent heat flux profiles at eight locations over Rattlesnake Mountain at 2300 PST 1 July 1980.

forcing of anisotropy, as shown in Eq. (2). If the Reynolds stress is weak, the anisotropy generated by the turbulent heat flux can dominate. This is the second mechanism responsible for the increase in $\overline{w'^2}/q^2$ as x increases over the leeward slope. As stated earlier, the

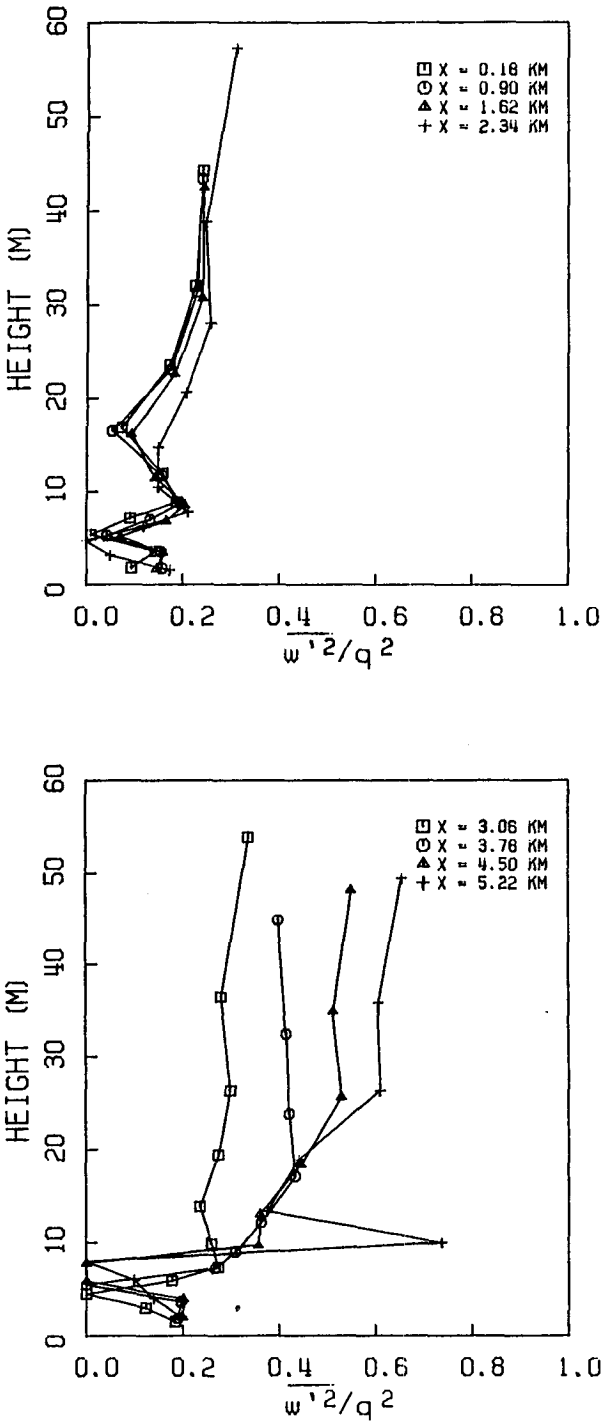

FIG. 9. Simulated profiles of the vertical component proportion of the TKE over Rattlesnake Mountain at 2300 PST 1 July 1980.

turbulent heat flux is comprised of a gradient portion and a countergradient portion given by $3l_2\beta g\overline{\theta_v' w'^2}/q$ [see Eq. (4)]. The increases in $\overline{w'^2}/q^2$ values occur at heights where the gradient portion of the vertical heat flux is small, as shown by the nearly adiabatic conditions above 12 m in Fig. 4. If the gradient portion of the vertical heat flux is small enough, the countergradient heat flux can force the total heat flux to become positive. This is evident in the heat flux profiles shown in Fig. 8. The countergradient heat flux causes the total heat flux to be quite erratic in the inversion layer, and to become positive and increase as x increases above the inversion layer. Upward heat fluxes in regions of weak mechanical production of turbulence anisotropy will tend to increase $\overline{w'^2}/q^2$ values beyond the isotropic limit.

5. Summary and conclusions

A two-dimensional second-order closure model based on level 3 of the Mellor–Yamada turbulence hierarchy has been applied to the Rattlesnake Mountain data for 1 July 1980 as an extension of the work of Yamada (1983). The model is used to simulate mean and turbulence quantities during nocturnal drainage flow conditions. Mean velocities and potential temperatures are examined for purposes of model verification and mean effects. Turbulence characteristics are examined in terms of variations in TKE, anisotropy, momentum fluxes, and heat fluxes.

The mean velocity profiles indicate the development of drainage layers over both the windward and leeward slopes of Rattlesnake Mountain. The ambient flow affects the strength and position of the katabatic flow maxima. The drainage layer grows with increasing distance from the ridge top over the leeward slope, indicating significant interfacial entrainment.

Simulated potential temperatures suggest enhanced stability over the leeward slope above the drainage flow maxima. Stability is less above the drainage flow maxima over the windward slope, suggesting increased turbulence there.

The TKE profiles reflect regions of increased mechanical production. Turbulence is reduced by about 50% over the leeward slope at a height where turbulence is at a maximum over the windward slope. The interaction of the vertical mean wind shear and the associated Reynolds stresses produces differences in the mechanical production of TKE over the windward and leeward slopes.

The turbulence field develops significant anisotropy near the surface where vertical wind shears and stability are large. Over the leeward slope above the drainage layer, anisotropy increases with increasing downslope distance. The vertical component proportion of the total TKE is enhanced in this region due to the countergradient portion of the heat flux. This countergradient process in stable conditions is dependent on the evolution of the virtual potential temperature variance field. The present simulation produces variances that are significantly larger above the drainage layer over

the leeward slope than over the windward slope. As a result, the anisotropy in the turbulence field above the drainage layer is larger over the leeward slope.

The results from the present study should be observed qualitatively in regions of significant turbulence anisotropy. The use of level 3 of the Mellor–Yamada hierarchy implies small departures from isotropy. However, the departures in this simulation are not small. This stretches the Rotta (1951) parameterization of pressure–velocity-gradient correlations that is used in level 3 of the Mellor–Yamada hierarchy to the limit of validity. Nevertheless, qualitative analysis of the results indicate anisotropic tendencies that should not be ignored in characterizing complex-terrain effects on the turbulence structure during stable conditions.

APPENDIX

List of Symbols

$A_1 = 0.92$ $A_2 = 0.74$ $C_1 = 0.08$	Constants of proportionality in Mellor–Yamada scheme
g	Acceleration of gravity
H	Height of model top
l	Master length scale for Mellor–Yamada scheme
$l_1 = A_1 l$ $l_2 = A_2 l$	Length scales for tendency toward isotropy in Mellor–Yamada scheme
q^2	$(\overline{u'^2} + \overline{v'^2} + \overline{w'^2})$
$q^2/2$	Turbulent kinetic energy
s	Height coordinate in the terrain-following coordinate system
U	Mean horizontal velocity in x direction
U_g	Geostrophic velocity in x direction
u'	Horizontal perturbation velocity in x direction
u_*	Friction velocity
V	Mean velocity in y direction
V_g	Geostrophic velocity in y direction
v'	Horizontal perturbation velocity in y direction
w'	Vertical perturbation velocity in z direction
x, y	Horizontal Cartesian coordinates
z	Vertical Cartesian coordinate
z_g	Height of the ground above some reference height
z_0	Roughness length
β	Coefficient of thermal expansion
Θ_v	Mean virtual potential temperature
θ'_v	Perturbation virtual potential temperature

REFERENCES

Arritt, R. W., and R. A. Pielke, 1986: Interactions of nocturnal slope flows with ambient winds. *Bound.-Layer Meteor.*, **37,** 183–195.

Bader, D. C., T. B. McKee and G. J. Tripoli, 1987: Mesoscale boundary layer evolution over complex terrain. Part I: Numerical simulation of the diurnal cycle. *J. Atmos. Sci.*, **44,** 2823–2838.

Businger, J. A., J. C. Wyngaard, Y. Izumi and E. F. Bradley, 1971: Flux-profile relationships in the atmospheric surface layer. *J. Atmos. Sci.*, **28,** 181–189.

Chang, L. P., E. S. Takle and R. L. Sani, 1982: Development of a two-dimensional finite-element PBL model and two preliminary model applications. *Mon. Wea. Rev.*, **110** 2025–2037.

Clements, W. E., J. A. Archuleta and D. E. Hoard, 1989: Mean structure of the nocturnal drainage flow in a deep valley. *J. Appl. Meteor.*, **28,** 457–462.

Deardorff, J. W., 1978: Efficient prediction of ground surface temperatures and moisture with inclusion of a layer of vegetation. *J. Geophys. Res.*, **83,** 1889–1904.

Doran, J. C., M. L. Wesely, R. T. McMillen and W. D. Neff, 1989: Measurements of turbulent heat and momentum fluxes in a mountain valley. *J. Appl. Meteor.*, **28,** 438–444.

——, and T. W. Horst, 1983: Observations and models of simple nocturnal slope flows. *J. Atmos. Sci.*, **40,** 708–717.

Garrett, A. J., 1983: Drainage flow prediction with a one-dimensional model including canopy, soil, and radiation parameterizations. *J. Climate Appl. Meteor.*, **22,** 79–91.

——, and F. G. Smith III, 1984: Two-dimensional simulations of drainage winds and diffusion compared to observations. *J. Climate Appl. Meteor.*, **23,** 597–610.

Gudiksen, R. H., Ed., 1983: ASCOT data from the 1980 field measurement program in the Anderson Creek Valley, California. ASCOT-83-1, Vol. 1, Lawrence Livermore National Laboratory, Livermore, CA, 537 pp.

Heilman, W. E., 1984: A one-dimensional numerical simulation of the boundary layer features over a uniformly vegetated sloping surface. M. S. thesis, Iowa State University, 236 pp.

——, 1988: Two-dimensional numerical simulations of the turbulence characteristics over Rattlesnake Mountain during stable and unstable conditions. Ph.D. dissertation, Iowa State University, 135 pp.

——, and R. Dobosy, 1985: A nocturnal atmospheric drainage flow simulation investigating the application of one-dimensional modeling and current turbulence schemes. *J. Climate Appl. Meteor.*, **24,** 924–936.

Horst, T. W., and J. C. Doran, 1982: Simple nocturnal slope flow data from the Rattlesnake Mountain site. ASCOT-82-5, Pacific Northwest Laboratory, Richland, WA, 98 pp.

——, and ——, 1986: Nocturnal drainage flow on simple slopes. *Bound.-Layer Meteor.*, **34,** 263–286.

——, and ——, 1988: The turbulence structure of nocturnal slope flow. *J. Atmos. Sci.*, **45,** 605—616.

Kasahara, A., 1974: Various vertical coordinate systems used for numerical weather prediction. *Bound.-Layer Meteor.*, **21,** 341–356.

Leone, J. M., Jr., and R. L. Lee, 1989: Numerical simulation of drainage flow in Brush Creek, Colorado. *J. Appl. Meteor.*, **28,** 530–541.

Manins, P. C., and B. L. Sawford, 1979a: A model of katabatic winds. *J. Atmos. Sci.*, **36,** 619–630.

——, and ——, 1979b: Katabatic winds: A field case study. *Quart. J. Roy. Meteor. Soc.*, **105,** 1011–1025.

McNider, R. T., and R. A. Pielke, 1984: Numerical simulation of slope and mountain flows. *J. Climate Appl. Meteor.*, **23,** 1441–1453.

Mellor, G. L., and T. Yamada, 1974: A hierarchy of turbulence closure models for planetary boundary layers. *J. Atmos. Sci.*, **31,** 1791–1806.

Nappo, C. J., Jr., and K. S. Rao, 1987: A model study of pure katabatic flows. *Tellus*, **39A,** 61–71.

Nieuwstadt, F. T. M., 1984: The turbulent structure of the stable, nocturnal boundary layer. *J. Atmos. Sci.*, **41,** 2202–2216.

Polezhaev, V. I., 1967: Numerical solution of the system of two-dimensional unsteady Navier–Stokes Equations for a compressible gas in a closed region. *Fluid Dyn.*, **2,** 70–74.

Rao, K. S., and H. F. Snodgrass, 1981: A nonstationary nocturnal drainage flow model. *Bound.-Layer Meteor.*, **20,** 309–320.

Rotta, J. C., 1951: Statistische Theorie Nichthomogener Turbulenz. *Z. Phys.*, **129,** 547–572.

Shinn, J. H., R. T. Cederwall, F. J. Gouveia and K. R. Chapman, 1989: Micrometeorology of slope flows in a tributary canyon during the 1984 ASCOT experiment. *J. Appl. Meteor.*, **28,** 569–577.

Song, J. L., R. A. Pielke, M. Segal, R. W. Arritt and R. C. Kessler, 1985: A method to determine nonhydrostatic effects within subdomains in a mesoscale model. *J. Atmos. Sci.*, **42,** 2110–2120.

Stone, G. L., and D. E. Hoard, 1989: Low-frequency velocity and temperature fluctuations in katabatic valley flows. *J. Appl. Meteor.*, **28,** 477–488.

Whiteman, C. D., and S. Barr, 1986: Atmospheric mass transport by along-valley wind systems in a deep Colorado valley. *J. Climate Appl. Meteor.*, **25,** 1205–1212.

Yamada, T., 1975: The critical Richardson number and the ratio of the eddy transport coefficients obtained from a turbulence closure model. *J. Atmos. Sci.*, **32,** 926–933.

——, 1981: A numerical simulation of the nocturnal drainage flow. *J. Meteorol. Soc. Jpn.*, **59,** 108–122.

——, 1983: Simulations of nocturnal drainage flows by a q^2–l turbulence closure model. *J. Atmos. Sci.*, **40,** 91–106.

——, and S. Bunker, 1989: A numerical model study of nocturnal drainage flows with strong wind and temperature gradients. *J. Appl. Meteor.*, **28,** 545–554.